This paper has been accepted for publication in Composites Part A

An Experimental Study of Scaling Effects in Notched Quasi-isotropic Carbon/Epoxy Laminates under Compressive Loads

Xiaodong Xu*, Aakash Paul, Xiaoyang Sun, Michael R. Wisnom

Bristol Composites Institute (ACCIS), University of Bristol, University Walk, Bristol BS8 1TR, UK

ABSTRACT

The size effects in centre-notched quasi-isotropic carbon/epoxy laminates under compression were investigated. The in-plane dimensions of the baseline specimen were scaled up by a factor of up to 14. The centre-notched specimens were compared to open-hole specimens of the same dimensions. It was found that compressive strength of the small centre-notched specimen is similar to that of the open-hole specimen. However, as the in-plane dimensions increase, the centre notches are weaker than the open holes, and start to follow a Linear Elastic Fracture Mechanics (LEFM) scaling line. These trends were well captured by a Composite Compressive Strength Modeller (CCSM) using the fracture energy measured in the current study. Fibre micro-buckling was confirmed to be the dominant failure mechanism under compression. The failure mechanisms under compression were also compared against those under tension. Matrix splitting under compression was observed through X-ray Computed Tomography but was less extensive than under tensile loading.

Keywords: A. Laminate; B. Strength; B. Fracture; D. CT analysis; Scaling effect

1. INTRODUCTION

Compressive strength of composite materials is of primary importance for designers. Budiansky and Fleck [1] considered compression as a critical case which needs to be understood. They reported that the typical failure mechanism for an

*Corresponding author.
E-mail address: xiaodong.xu@bristol.ac.uk (X. Xu).

unnotched unidirectional composite specimen under compression is by plastic kinking (local fibre micro-buckling). The kinking mechanism is sensitive to fibre misalignment which can occur during manufacturing, resulting in plastic shear deformation in the matrix when applying compressive loads. Wisnom [2] reviewed compression tests to investigate the variation in strength as the size of the unnotched specimen increases. The effects of manufacturing were highlighted. It was concluded that the scaling effect of compressive strength in composites is significant.

The reduction in the compressive strength due to the introduction of notches makes this a key driver when designing composite structures. Stress concentrations can arise from cut-outs, bolted joints or impact damage which can have detrimental effects on composite structures. There has been extensive research within this field to understand how scaling effects influence the compressive failure of open-hole composites. Bažant et al. [3] investigated unidirectional notched carbon–PEEK composites, failing by propagation of a kink band with fibre micro-buckling. They demonstrated that the strength scaling line for large notched specimens with a long kink band approaches an asymptote of slope −1/2 (characteristic of Linear Elastic Fracture Mechanics, LEFM) on the bi-logarithmic plot of the nominal strength vs. the characteristic size. Lee and Soutis [4] studied the failure mechanism of an open-hole quasi-isotropic specimen under compression while also investigating the size effects. They concluded that the failure was dominated by the presence of the hole, driving delamination and fibre micro-buckling along the plane of fracture in the vicinity of the hole. Wisnom et al. [5] summarized the strength scaling for sub-laminate scaled and ply-level scaled open-hole specimens under both tension and compression, demonstrating strong size effects under both loading conditions. Erçin et al. [6] also

studied the effects of size on open-hole specimens under both tension and compression. They reported that the open-hole compressive strengths decrease faster than the open-hole tensile strengths with the same diameters ranging from 3 to 7 mm for a $[90/45/0/-45]_{3s}$ laminate. When comparing open-hole tension and compression test results, the open-hole tensile strengths were 66-91% higher than the open-hole compressive strengths with a greater difference for the largest specimens. Although no damage was observed prior to the peak load in the open-hole compression tests using Aramis Digital Image Correlation (DIC) system, sub-critical failure mechanisms were expected to have caused the size effect. The authors also applied Finite Fracture Mechanics models that have proven to be able to capture both the open-hole and centre-notched tensile and compressive failure [6]. However, the details of the sub-critical failure mechanisms under compression were not discussed. Few studies were found on compressive strength scaling for centre-notched quasi-isotropic laminates in the literature. Although Tan et al. [7] conducted experiments on relatively small quasi-isotropic specimens both with a sharp centre notch and an open hole under compression, no centre-notched or open-hole specimens of other sizes were tested. Furthermore, few studies compared the centre-notched failure under compression against the behaviour under tension.

Soutis et al. [8] developed a theoretical model to predict the notched strength of open-hole specimens and the critical micro-buckling length at failure. This model was derived from models [9, 10] originally developed for metals under tension, which were then modified for composites under compression. The micro-buckled region was modelled as a crack, over which the normal traction acting on the crack flanks was assumed to decrease linearly with the crack normal displacement. The correlation of the predicted open-hole results from the model and experimental results was very strong.

This method has been integrated into a Composite Compressive Strength Modeller (CCSM) [11]. Other progressive damage modelling tools have been introduced to predict the strengths and failure patterns in open-hole specimens. For example, Su et al. [12] developed a progressive damage model for open-hole composite laminates under compression. They did not explicitly model the fibre micro-buckling, which was represented by a linear softening law instead. Under compression, instability and local buckling were problems that led to convergence issues. This was mitigated using a zigzagging softening curve developed by Ridha et al. [13], which always maintains a positive tangent modulus in the stress–strain curve. Pinho et al. [14] developed a smeared crack model, in which the total energy dissipated was proportional to the micro-buckling length propagation. The strain energy dissipated during the micro-buckling was mesh-independent as per the cohesive law embedded in this model. Ortega et al. [15] adopted an inverse approach to characterize the trans-laminar cohesive laws under both tensile and compressive loads. They compared different stacking sequences and materials, and highlighted the stress blunting effect of the blocked plies in the loading direction. They did not explicitly model the fibre micro-buckling either but derived a cohesive law to represent the micro-buckling process under compressive loads.

The present paper presents the scaling effect in centre-notched quasi-isotropic laminates under compressive loads. This was achieved by testing centre-notched specimens scaled in-plane by a factor of up to 14, with a constant notch-to-width ratio and laminate thickness. The Composite Compressive Strength Modeller (CCSM) [11] using the fracture energy measured in the current study has been used to predict the scaling effects with satisfactory accuracy. Some further examinations were made to

explain the development of the micro-buckling lengths, in which tests were interrupted at about 95% of the average failure load, and then X-ray Computed Tomography (CT scan) was conducted to analyse the internal damage prior to ultimate failure. For the first time centre-notched compression test results were compared to open-hole compression test results with the same material and specimen dimensions over a range of sizes. To form a full comparison, some very small and large open-hole specimens were also conducted in addition to the previous open-hole results from Lee and Soutis [4]. The failure mechanisms and scaling in both the open-hole and centre-notched compression tests were also compared with those in previous tension tests [16].

2. EXPERIMENTAL SETUP

2.1 Specimen configurations

The schematic of all centre-notched specimen used is shown in Figure 1, where *W*, *L* and *C* represents the specimen width, length and notch length respectively. The in-plane dimensions of the smaller specimens (*C* = 3.2, 6.35, 12.7 and 20 mm) are scaled as per Figure 1a. The Scale 8 specimens (*C* = 25.4 mm) were tested with reduced gripping area as shown in Figure 1b because of the limited width of the grips on the test machine. There is an even larger set of Scale 14 specimens (*C* = 45 mm) tested with no gripping sections as shown in Figure 1c because they were end loaded on the edges. Table 1 summarizes the specimen dimensions of all different scales.

The material used for all experiments was Hexcel's HexPly© IM7/8552 carbon/epoxy pre-preg with a nominal ply thickness of 0.125 mm. Experiments were conducted on a quasi-isotropic stacking sequence of $[45/90/-45/0]_{4s}$. The laminate thickness of 4 mm was constant for all tests, and the measured thicknesses were very close.

The through-the-thickness centre notches were cut by using a Computer Numerical Controlled (CNC) machine. The notch tip radius was 0.5 mm, driving the notch width to be 1.0 mm to avoid crack closure under compressive loading, but still inducing high stress concentration factors at the tips. This was similar to that in Tan et al. [7] in which a notch radius of 0.35 mm was used. The notch radius was held constant for all specimens.

Open-hole specimens were also tested to compare to the centre notches. The smaller holes (3.2 and 6.4 mm [4]) were cut using carbide drill bits. The previous [4] (12.7 and 25.4 mm) and the current (20 and 45 mm) larger holes were cut using diamond coated hollow drill bits. The hole diameters were kept the same as the centre-notch lengths, while the other specimen dimensions were also identical.

2.2 Test configurations

An Instron hydraulically driven machine was used for the experiments. The loading rate during the experiments was scaled as the in-plane dimensions increased, starting at 0.125 mm/min for the baseline specimen, and scaled up with the gauge length. The specimens in Figure 1a and b were directly gripped in the test machine as illustrated in Figure 2a and 2b. However, the largest Scale 14 specimens (Figure 1c) were tested differently because they were too wide for the steel jaws of the test machine. Therefore the specimens were tested in a Compression after Impact (CAI) jig [17] and end loaded by a pair of steel half rods which are flattened where they touch the specimen and connected to the test machine (Figure 2c). Due to the increased gauge length, the stress at which the specimen buckles decreases. Anti-buckling guides were therefore introduced in the larger Scale 6, Scale 8 (Figure 2b) and Scale 14 tests (Figure 2c) but were found not necessary in smaller baseline, Scale 2, Scale 4 tests (Figure 2a).

For the Scale 8 specimens, steel anti-buckling guides were applied at either side of the specimen, gently clamping the specimen gauge section in the loading direction using two knife edges on each side. Two G clamps were also used to limit the horizontal movement of the jig, ensuring that it remained still during the experiments. The hydraulic grips were then applied on both the upper and lower gripping sections of the specimen. This jig proved to be successful, as no buckling was observed during testing. A typical load vs. crosshead displacement curve from a Scale 8 compression test is illustrated in Figure 3a. The grips on the Instron machine were limited to 100 mm width, but the Scale 8 specimen has a width of 127 mm. As the gripping width is smaller than the specimen width and the specimens slightly protruded at the sides of the gripping region, the load at the grips was applied over a smaller width as shown in Figure 1b. The resulting stress distribution was checked in a linear elastic FE analysis to ensure even loading condition across the specimen width at the notch location. Another single Scale 6 experiment was also conducted to further validate the Scale 8 experimental results. These will be explained later.

The largest Scale 14 tests were even more challenging. Because the specimen width (225 mm) is much wider than the width of the grips (100 mm), the specimens (Figure 1c) were not directly gripped in the test machine but loaded at the top and bottom edges in a CAI jig. Two chamfered semi-cylindrical rods were assembled into a pair of anti-buckling guides, and the upper one was driven by a steel plate which was clamped onto the test machine as shown in Figure 2c. Initially, this configuration was found to be problematic because global buckling still occurred at the notch. A further improvement was made by covering the specimens with two 3-mm thick Aluminium plates to reinforce the specimen surfaces and stop global buckling. Friction introduced

by the Aluminium plates is considered to be negligible because the clamping force at the bolts is small. This was proven to be effective for the centre notches with trans-laminar fracture starting from the notch tips visible on both specimen surfaces. However, this did not work for the open holes, which showed trans-laminar fracture starting from the hole edge on one specimen surface and delamination from other, which indicates global buckling. As a result, the Scale 14 open-hole results were discarded.

Interrupted tests were conducted at around 95% of the average failure load measured for the baseline (C = 3.2 mm), Scale 2 (C = 6.4 mm), Scale 4 (C = 12.7 mm) and Scale 8 (C = 25.4 mm) centre-notched specimens. The specimens for CT scans were soaked in zinc iodine X-ray penetrant solution for 2 days before CT scans were done using a Nikon XTH225ST CT scanner, with a 3 μm focal spot size and 225 kV, 225 W microfocus X-ray source. The largest Scale 14 specimens were not scanned because of the limited number of specimens and the fact that CT scanning would not yield sufficient resolution for the largest specimens.

2.3 Simple FEA to verify Scale 8 specimens

Four-noded shell elements with isotropic homogenized properties were used to represent a quarter of the Scale 8 centre-notched specimen, taking advantage of the symmetric in-plane geometry and loading condition. Symmetry boundary conditions were used at the two mid-planes of the full-scale model, and a unit compressive stress was applied to the boundary of the specimen gauge section in the loading direction. The gripping section of the specimen was also modelled where all degrees of freedom were constrained except for the translation along the loading direction. The size of the mesh at the notch tip was 0.5 mm with an aspect ratio of 1. The stress at the notch tip was

bound to be mesh-dependent since the sharp crack produces a stress singularity, so only used here for comparison purposes. The first case examined was a unit compressive stress applied over the full width. The second case examined was for narrow grips, where the same load was applied to a narrower 100 mm width section in the middle of the specimen. The stress distribution across the specimen half width is similar in both cases in terms of the stress concentration factor (elemental stress over the applied unit stress) as shown in Figure 4, with a difference of less than 3.5%. This confirmed that narrow grips do not significantly affect the stress distribution at the notch tips.

3. TEST RESULTS

3.1 Results summary

Table 2 presents the test results obtained for the notched specimens under compression for different specimen sizes. The strength values were taken as the gross-section stress from the load vs. displacement graph at ultimate failure. The displacements were measured at the crosshead. The load vs. crosshead displacement curves of the specimens of different sizes have a similar shape. There are no load drops until sudden failure as shown in Figure 3a. The response is initially fairly linear until ultimate failure. Some non-linear response was found in the smallest baseline specimens due to slippage at the grips and the largest Scale 14 specimens due to compliance in the fixture. The ultimate failure observed for all centre-notched specimens was catastrophic, with a similar fracture morphology parallel to the centre notch across the width as shown in Figure 3b. The photograph of the smallest failed baseline specimen is used to give the best image quality around the notch across the width. Scale 14 open-hole specimens buckled before ultimate failure, so the results are not comparable in Table 2.

3.2 Extra test to verify Scale 8 results

Another single Scale 6 centre-notched experiment was also conducted to further validate the Scale 8 centre-notched experimental results. Keeping the notch-to-width ratio of 0.2 consistent with the other experiments, a centre notch length of C = 20 mm was cut for a 100 mm wide specimen which is the maximum for the grips on the Instron test machine. The single test result was found to follow the trend obtained with the other experimental results as shown in Figure 5. This indicated that narrow grips do not have a significantly effect.

3.3 Observed scaling effect

There is a strong scaling effect for the centre-notched strengths as shown in Figure 5 and the results listed in Table 2. The compressive strengths decrease with increasing specimen dimensions. The open-hole strengths follow a similar scaling trend at the smaller sizes but start to deviate from the Scale 8 results. However, it is less conclusive due to the absence of the largest Scale 14 result because of buckling.

4. DEVELOPMENT OF MICRO-BUCKLING

The development of micro-buckling in the baseline, Scale 2, Scale 4 and Scale 8 specimens was examined by conducting CT scans of one specimen interrupted at 95% of the average failure load for each case. The purpose is to examine the damage state at the notch tip just before ultimate failure. Detailed information about fibre micro-buckling at the notch tip is the key to understanding notched compression failure.

4.1 Baseline specimen (C = 3.2 mm)

CT scan images of the baseline specimen from the interrupted tests at about 95% of the average failure load are shown in Figure 6. At the outboard single 0° plies through the thickness of the baseline specimen, fibre micro-buckling is observed at the

edge of the notch. The fibre micro-buckling does not appear in the central 0° plies where two plies are blocked together as seen in Figure 6d. This is because of the long 0° splitting (Figure 6d) at the specimen mid-plane which can blunt the stress concentration and delay the initiation of the micro-buckling. A small amount of splitting was also visible in nearly all ±45° plies through the specimen thickness as shown in Figure 6a and 6b, but there was no obvious fibre micro-buckling in these plies. In the typical outboard 0° plies, shown in Figure 6c, fibre micro-buckling grows at a kink angle β of 38° in this case. No splits were observed in the outboard single 0° plies. There is hardly any visible damage under compression in the 90° plies.

4.2 Scale 2 specimen (C = 6.4 mm)

In Figure 7, CT scans of the typical plies for the Scale 2 specimen from the interrupted tests at 95% of the average failure load are shown. Fibre micro-buckling is only observed at one edge of the notch in the central double 0° ply, as seen in Figure 7d, compared to both sides in the baseline specimen. This is consistent with the observations in Lee and Soutis [4] for the open-hole specimen of the same size from an interrupted test at 98% of the average failure load. This could be because of matrix splitting being present on one side of the notch in the central double 0° ply block, which can delay the onset of micro-buckling initiation on that side. Splitting was also visible in nearly all ±45° plies through the specimen thickness as shown in Figure 7a and 7b, with no fibre micro-buckling. In the typical outboard 0° plies, shown in Figure 7c, fibre micro-buckling grows at a kink angle β of 31° in this specimen. There were no splits in the single 0° plies. The fibre micro-buckling length in the outboard single 0° plies is smaller when compared to that in the central double 0° ply block. There is again hardly any visible damage under compression in the 90° plies.

4.3 Scale 4 specimen (C = 12.7 mm)

The main difference between the Scale 2 and Scale 4 specimens is that the fibre micro-buckling is observed on both sides of the central double 0° ply with the presence of 0° splitting as shown in Figure 8d. This fibre micro-buckled region is at a kink angle β of 31°. There are also some delaminations present in the outboard 0° plies near the specimen surfaces. The length of the fibre micro-buckled region is longer than that in the baseline specimen. The splitting in the ±45° plies is similar to that in the baseline specimen. Again, there is hardly any visible damage under compression in the 90° plies.

4.4 Scale 8 specimen (C = 25.4 mm)

The Scale 8 fibre micro-buckling length at the central double 0° plies is larger compared to the Scale 4 specimen, as shown in Figure 9d. The fibre micro-buckled region is at a kink angle of β of 24° in this case. Delaminations are present again in some outboard 0° plies near the specimen surfaces. The splitting in the ±45° plies is similar to the other three sizes analysed. No obvious damage was observed in the 90° plies under compression.

4.5 Comparison of fibre micro-buckling lengths

The fibre micro-buckling lengths from the tests interrupted at about 95% average failure loads were measured. The maximum absolute length in the 0° plies and on both sides of the centre notch was taken to estimate the critical micro-buckling length at ultimate failure. In Reference [5] micro-buckling length was measured from the X-ray scan images taken at 98% of the average failure load. Since the damage in the different plies through the specimen thickness overlaps in the 2D X-ray images, the fibre micro-buckling length reported is presumably the maximum value which is the same as in the current study. The maximum values for the fibre micro-buckling lengths are 1.6 mm,

2.2 mm, 2.6 mm and 2.8 mm for baseline, Scale2, Scale 4 and Scale 8 specimens respectively. The measured micro-buckling lengths seem to be approaching a plateau, which indicates that Linear Eleatic Fracture Mechanics (LEFM) should apply to the scaling of very large centre-notched strengths.

5. RESULTS ANALYSIS

5.1 Linear Elastic Fracture Mechanics (LEFM)

In the current study, a trans-laminar fracture toughness K_C = 43.9 MPa·m$^{0.5}$ can be calculated from the largest Scale 14 centre-notched compression tests according to Equation 1[10].

$$K_C = \sigma_n f(\lambda) \sqrt{\frac{\pi C}{2}} \tag{1}$$

where σ_n is the average nominal gross-section strength, from the largest Scale 14 compression tests, $\sigma_{n\_\text{Scale14}}$ = 161 MPa, and C = 45 mm is the crack length, $f(\lambda) = \sqrt{\sec(\pi\lambda)}$ is a geometric parameter to account for the effect of finite width and $\lambda = C/2W$ is the equivalent half notch-to-width ratio and W is the specimen width.

The compressive strengths for different notch lengths calculated according to Equation 1 are plotted against the experimental results as shown in Figure 10. The predicted centre-notched strengths correlate reasonably well with the large test results (Scale 4, Scale 8 and Scale 14). This supports the applicability of LEFM for large centre-notch specimens.

5.2 Composite Compressive Strength Modeller (CCSM)

Sutcliffe et al. [11] developed a Composite Compressive Strength Modeller (CCSM) which is a software design tool for deformation analysis and failure prediction of composite materials. Its compressive failure prediction tool for open hole composite

plates is developed from Soutis et al. [8], which assumes a crack-like micro-buckling mechanism grows from the edge of the hole. Over the micro-buckling zone, a bridging law exists which assumes that the traction reduces linearly in proportion to the crack closure from the unnotched compressive strength to zero, and the area under the traction vs. closure line is the fracture energy [8]. Furthermore, a number of bridging analyses have been carried out based on Sutcliffe and Fleck [18] for different types of commonly used notched specimens e.g. centre-notched and open-hole specimens, and for a range of crack and ligament sizes. Results are expressed as a function of a/r_p and b/r_p, where a and b are crack length and ligament length respectively; and r_p is a bridging scale, and σ_u is the unnotched strength given as:

$$r_p = \frac{K_C^2}{\sigma_u^2} \tag{2}$$

CCSM utilises the look-up tables [18] to interpret the notched strength and micro-buckling length of centre notched specimens. The look-up tables consist of contour or surface plots of the independent variables (including critical micro-buckle length, remote stress and stress intensity factor at failure). As such, the effect of large-scale bridging can be summarised onto one graph. It should be noted that the look-up tables used for strength predictions are valid only when the specimen and crack length fit within certain geometry constraints. The stress intensity factor caused by the remote stress K_r and critical micro-buckling length l_C must be within the limits. Once outside the limits, an extrapolation technique needs to be used which relies on some asymptotic functions. The limit relevant to the current study quoted from the user's manual for CCSM [11] is:

$$a/r_p \gg 1 \text{ and } b/r_p \gg 1 \tag{3}$$

Centre-notch: $K_r \rightarrow K_C$, $l_C \rightarrow 0.75r_p$, $\sigma_n = K_r/(f(\lambda)\sqrt{\pi a})$

Open-hole: $l_C \rightarrow 0$ (unstable), $\sigma_n = \sigma_u/K_t$

(K_t is the stress concentration factor)

The main input parameters for the CCSM analysis are listed in Table 3. The trans-laminar fracture toughness K_C = 43.9 MPa·m$^{0.5}$ is taken from the largest Scale 14 centre-notched tests. The unnotched strength σ_u = 675 MPa is from [5]. The notched strengths predicted by CCSM are also shown in Figure 10. The predicted notched strengths agree reasonably well with all the experimental results except for the second largest Scale 8 notches which are underestimated. For larger sizes, the CCSM results also predict that the centre-notched results approach an LEFM scaling line, which is consistent with the experimental observations. Another output from the CCSM analysis for the centre-notched cases is the critical micro-buckling length at unstable compressive failure. The predicted critical micro-buckling lengths for centre notches are compared against the measured maximum values from CT scans at about 95% of the average failure loads in Figure 11. The correlation is reasonable, particularly at the large scales. This adds to the credibility of the CCSM predictions. The discrepancies in micro-buckling lengths may be partially attributed to the difference in load levels between the predicted critical micro-buckling lengths at failure (100%) and the measured values from CT scans at 95 % of the average failure loads. A small increment of applied load could lead to a large increment of micro-buckling length as implied in [8]. The predicted critical micro-buckling lengths for open holes are also shown in Figure 11.

The CCSM prediction tool [11] for notched composite plates has proven to be effective in predicting scaling of open-hole and centre-notched strengths. The fracture

toughness of K_C = 43.9 MPa·m$^{0.5}$ was directly calculated from the current largest Scale 14 centre-notched test. This is believed to be more accurate than taking it as the product of the unnotched strength and the half micro-buckling width as in the analytical model proposed in [8], which yields K_C = 40.8 MPa·m$^{0.5}$ (27 kJ/m^2 [5]) for the same material and stacking sequence. If K_C = 40.8 MPa·m$^{0.5}$ was taken as the fracture toughness, the predictions would be conservative for larger notched specimens.

5.3 Comparison with open-hole results

Figure 10 demonstrates how the centre-notched results differ from open holes.

From the baseline to the Scale 4 specimens, there is no significant difference between the open-hole and centre-notched strengths. The failure mechanism is also similar, which is fibre micro-buckling in the 0° plies. Consequently, the difference in notched strengths between the centre notch and the open hole is small. CCSM predicts that the open holes are only slightly stronger than the centre notches from the baseline to the Scale 8 specimens.

For the second largest Scale 8 specimens, there is a significant difference between the specimens with centre notches and open holes, in which the latter are stronger. According to the CCSM predicted notched strengths in Figure 10, the open-hole results approach a different scaling line from the centre-notched results. The CCSM predicted critical micro-buckling lengths also start to differ significantly at Scale 8 between open holes and centre notches as shown in Figure 11. For the large open holes, the critical fibre micro-buckling length does not grow with the hole radius but actually drops, as shown in Figure 11, leaving the critical fibre micro-buckling relatively much smaller than the hole radius. The strengths therefore are expected to tend towards being controlled by the unnotched strength of the laminate divided by the stress concentration

factor of 3.13 [19] (asymptote value of 216 MPa). However, this could not be verified due to global buckling issues with the largest open-hole specimens. This will be explained later. For the large centre notches, the CCSM predicted critical micro-buckling lengths grow with the notch lengths as shown in Figure 11, and are approaching a constant value that is still relatively small compared to the largest notch length of 45 mm. Therefore the centre-notched strengths tend to follow LEFM.

The largest Scale 14 open-hole results are not shown in Figure 10. This is because the results were influenced by premature buckling at the hole. This was found unavoidable with the existing experimental set-up. In contrast, the largest Scale 14 centre-notched tests were successful and validate the LEFM strength scaling based on the trend from the largest Scale 14 centre-notched results, as shown in Figure 10.

5.4 Stacking sequence effects

It is also interesting to consider stacking sequence effects, including the effect of ply thickness on notched compressive strength. For example, Lee and Soutis [4] studied the open-hole compressive strength scaling of dispersed-ply $[45/90/-45/0]_{4s}$ and blocked-ply $[45_4/90_4/-45_4/0_4]_s$ IM7/8552 carbon/epoxy laminates. They showed that both sets of quasi-isotropic laminates gave a reduction of open-hole compressive strength with increasing in-plane dimensions, with more strength reduction in the blocked-ply $[45_4/90_4/-45_4/0_4]_s$ laminates. The smaller specimens with blocked plies were found to be stronger than those with dispersed plies, though strengths were similar for the larger specimens. This was attributed to the stress redistribution due to 0° splitting around the hole in the blocked-ply laminates. Paul et al. [20] compared the centre-notched compressive strength between the dispersed-ply $[45/90/-45/0]_{4s}$ and $[90/45/0/-45]_{4s}$ IM7/8552 carbon/epoxy laminates, and found that both quasi-isotropic laminates

have the same notched compressive strength. The dominant failure mechanism was the same fibre micro-buckling, with little influence of 0° splitting with dispersed plies. These results suggest that the stacking sequence effect is not very significant unless plies are blocked.

5.5 Comparison with tensile test results

The failure mechanisms for centre-notched specimens are different under tension and compression. Under tension the key failure mechanism is local fibre breakage in the 0° plies forming a distinctive damage process zone with delamination and matrix splitting as shown in Figure 12 [16]. For small sizes, it was found that the centre-notched specimens are stronger in tension than the open-hole specimens. This is because of the presence of 0° splits which blunt the stress concentrations. There is a cross-over at a large notch length under tension between C = 25.4 and 50.8 mm when the damage process zone ahead of the large centre notch approaches a constant value, so its stress blunting effect is relatively small. Under compression, failure is dominated by fibre micro-buckling in the 0° plies. For small sizes, the centre notches have a similar strength compared with the open holes. A strength cross-over between the centre-notched and open-hole strengths can hardly be observed, because splitting is much less important in compression than tension. There is no splitting present in the outboard single 0° plies under compression compared with significant splits under tension as shown in Figure 12, resulting in much less stress blunting in the small centre notches in compression. The damage process zone under compression mainly consists of micro-buckling in the 0° plies. The micro-buckling length reaches 2.8 mm at Scale 8 which is comparable to the damage zone size of 2.3 mm under tension. However, it should be noted that the definition of damage process zone under tension is different from that

under compression. In both tension and compression the centre-notched strengths are asymptotic to a fracture mechanics scaling line, approaching it at similar specimen sizes. Based on the largest notched test results in each case, the measured fracture toughness value of K_C = 43.9 MPa·m$^{0.5}$ (G_C = 31.3 kJ/m^2) under compression is much lower than the value of K_C = 75.6 MPa·m$^{0.5}$ (G_C = 92.8 kJ/m^2) under tension [16].

6. CONCLUSIONS

The scaling effect of notched compressive strength in quasi-isotropic laminates was studied. The dominant failure mechanism under compression for both centre notches and open holes is fibre micro-buckling in the 0° plies initiating from the notch. CT scan images interrupted at about 95% of the average failure loads reveal that the fibre micro-buckling length is not a constant value but increases with notch length. The fibre micro-buckling does not grow parallel to the notch in the 0° plies, but at a kink angle β which is typically between 24° and 42° in the current quasi-isotropic laminate.

The notched compressive strength was found to decrease as the in-plane dimensions of the specimen increase, approaching a line consistent with LEFM scaling at the largest size. The centre-notched strength scaling was also compared to the open-hole strength scaling under compression. For smaller specimens, there was little difference in compressive strength between the centre-notched and open-hole specimen. However, as the notch length (hole diameter) increases to 25.4 mm the difference in strength significantly increases.

The CCSM analysis considering both fracture and strength properties effectively captures the strength scaling for the centre-notched and open-hole specimens. Based on the compressive strength value of 675 MPa [5] from the literature and the fracture toughness value of 43.9 MPa·m$^{0.5}$ measured from the largest Scale 14 tests for the

current IM7/8552 quasi-isotropic laminates, the CCSM predicted notched strengths and micro-buckling lengths agree reasonably well with almost all the experimental results.

Comparison was made between the centre-notched compressive and tensile failure mechanisms. Unlike fibre micro-buckling in the 0° plies for compression, the dominant failure mechanism for tension is the development of a damage process zone that consists of local fibre breakage in the 0° plies, splitting and delamination. Under compression, hardly any 0° splitting was observed except in the central double 0° plies at the initial notch tip, so it is less significant. In contrast, extensive multiple long splits were seen in all 0° plies under tension, playing a key role, and explaining the higher tensile strength for small centre notches compared to holes in tension, which was not observed in compression.

REFERENCES

[1] Budiansky B, Fleck NA. Compressive failure of fibre composites. Journal of the Mechanics and Physics of Solids. 1993;41(1):183-211.

[2] Wisnom MR. Size effects in the testing of fibre-composite materials. Composites Science and Technology. 1999;59(13):1937-57.

[3] Bažant ZP, Kim JH, Daniel IM. Size effect on compression strength of fiber composites failing by kink band propagation. International Journal of Fracture. 1999;95:103-41.

[4] Lee J, Soutis C. Measuring the notched compressive strength of composite laminates: Specimen size effects. Composites Science and Technology. 2008;68(12):2359-66.

[5] Wisnom MR, Hallett SR, Soutis C. Scaling effects in notched composites. J Compos Mater. 2010;44(2):195-210.

[6] Erçin GH, Camanho PP, Xavier J, Catalanotti G, Mahdi S, Linde P. Size effects on the tensile and compressive failure of notched composite laminates. Composite Structures. 2013;96:736-44.

[7] Tan JLY, Deshpande VS, Fleck NA. Failure mechanisms of a notched CFRP laminate under multi-axial loading. Composites Part A: Applied Science and Manufacturing. 2015;77(0):56-66.

[8] Soutis C, Fleck NA, Smith PA. Failure Prediction Technique for Compression Loaded Carbon Fibre-Epoxy Laminate with Open Holes. J Compos Mater. 1991;25(11):1476-98.

[9] Dugdale DS. Yielding of steel sheets containing slits. Journal of the Mechanics and Physics of Solids. 1960;8(2):100-4.

[10] Newman JC. Fracture analysis of various cracked configurations in sheet and plate materials. Properties Related to Fracture Toughness ASTM STP 605. 1976:104-23.

[11] Sutcliffe MPF, Xin XJ, Fleck NA, Curtis PT. Composite Compressive Strength Modeller. Version 2.0, 2013 ed. Cambridge, UK: Cambridge University; 2013. A Windows-based composite design tool for engineers.

[12] Su ZC, Tay TE, Ridha M, Chen BY. Progressive damage modeling of open-hole composite laminates under compression. Composite Structures. 2015;122:507-17.

[13] Ridha M, Wang CH, Chen BY, Tay TE. Modelling complex progressive failure in notched composite laminates with varying sizes and stacking sequences. Composites Part A: Applied Science and Manufacturing. 2014;58:16-23.

[14] Pinho ST, Iannucci L, Robinson P. Physically-based failure models and criteria for laminated fibre-reinforced composites with emphasis on fibre kinking: Part I:

Development. Composites Part A: Applied Science and Manufacturing. 2006;37(1):63-73.

[15] Ortega A, Maimí P, González EV, Sainz de Aja JR, de la Escalera FM, Cruz P. Translaminar fracture toughness of interply hybrid laminates under tensile and compressive loads. Composites Science and Technology. 2017;143:1-12.

[16] Xu X, Wisnom MR, Mahadik Y, Hallett SR. An experimental investigation into size effects in quasi-isotropic carbon/epoxy laminates with sharp and blunt notches. Composites Science and Technology. 2014;100(0):220-7.

[17] Weaver P, Potter K, Hazra K, Saverymuthapulle M, Hawthorne M. Buckling of Variable Angle Tow Plates: From Concept to Experiment. 50th AIAA/ASME/ASCE/AHS/ASC Structures, Structural Dynamics, and Materials Conference. California, US2009.

[18] Sutcliffe MPF, Fleck NA. Effect of geometry on compressive failure of notched composites. International Journal of Fracture. 1993;59(2):115-32.

[19] Xu X, Wisnom MR, Chang K, Hallett SR. Unification of strength scaling between unidirectional, quasi-isotropic, and notched carbon/epoxy laminates. Composites Part A: Applied Science and Manufacturing. 2016;90:296-305.

[20] Paul A, Xu X, Wisnom MR. An experimental investigation into the stacking sequence effects of quasi-isotropic carbon/epoxy laminates under compressive loads. 21st International Conference on Composite Materials. Xi'an, China 2017.

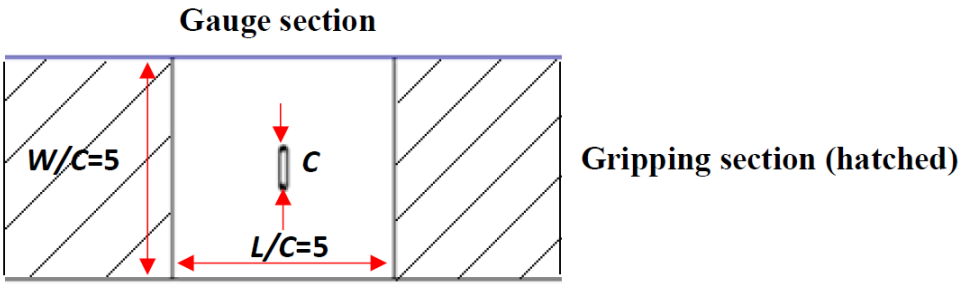

a) Fully gripped specimen geometry (C = 3.2, 6.4, 12.7 and 20 mm)

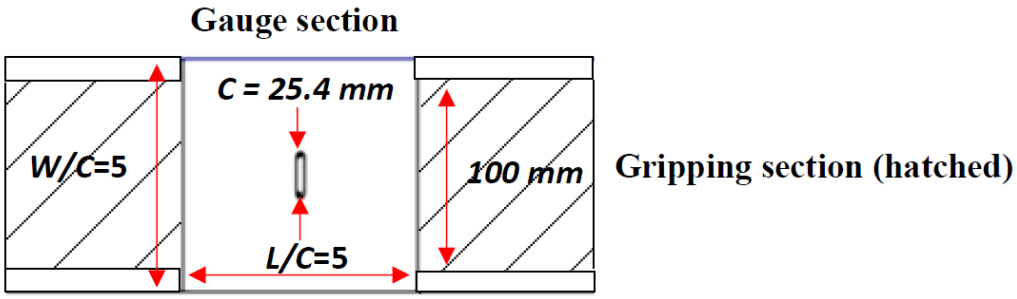

b) Partially gripped specimen geometry (C = 25.4 mm)

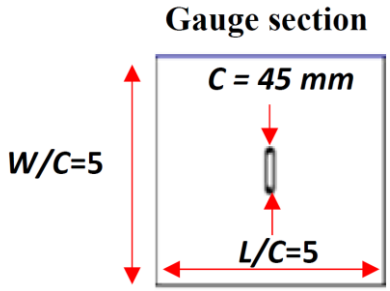

c) End loaded specimen geometry (C = 45 mm)

Figure 1. Schematics of the scaled specimens tested.

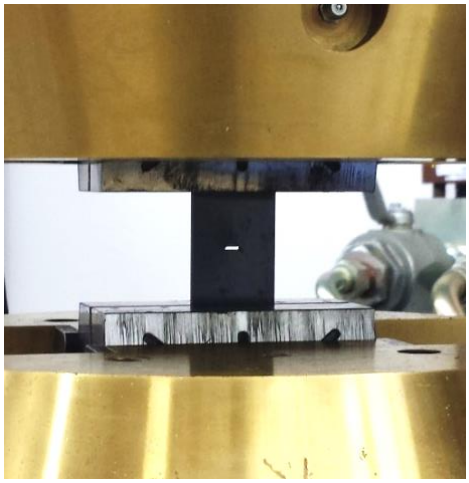

a) Fully gripped small specimens

(*C* = 3.2, 6.4 and 12.7 mm)

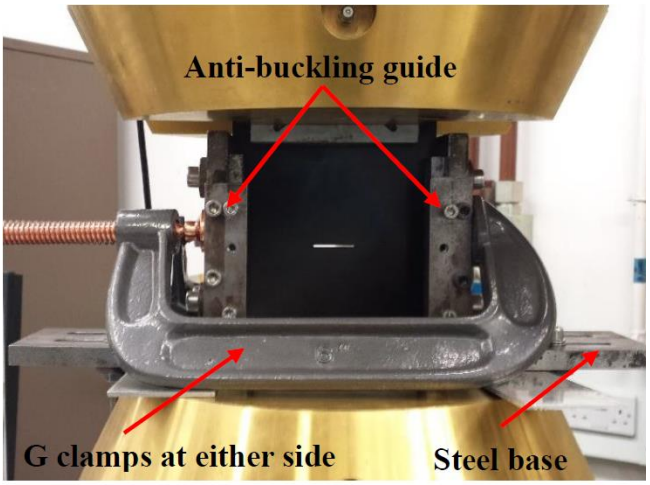

b) Gripped specimens with anti-buckling guides

(*C* = 20 and 25.4 mm)

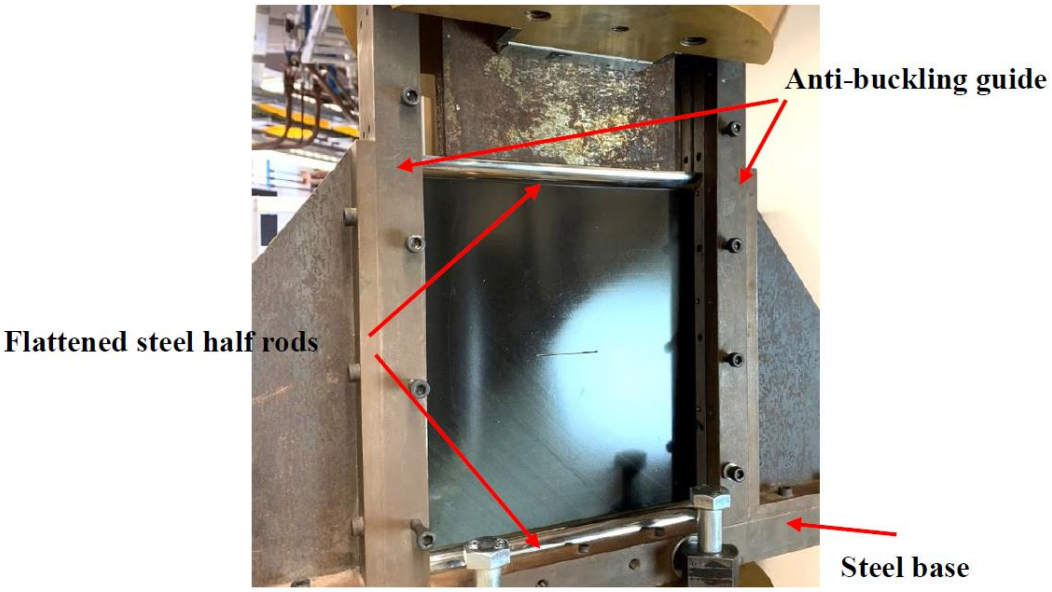

c) Largest end loaded specimen with anti-buckling guides (*C* = 45 mm)

Figure 2. Compression test configurations.

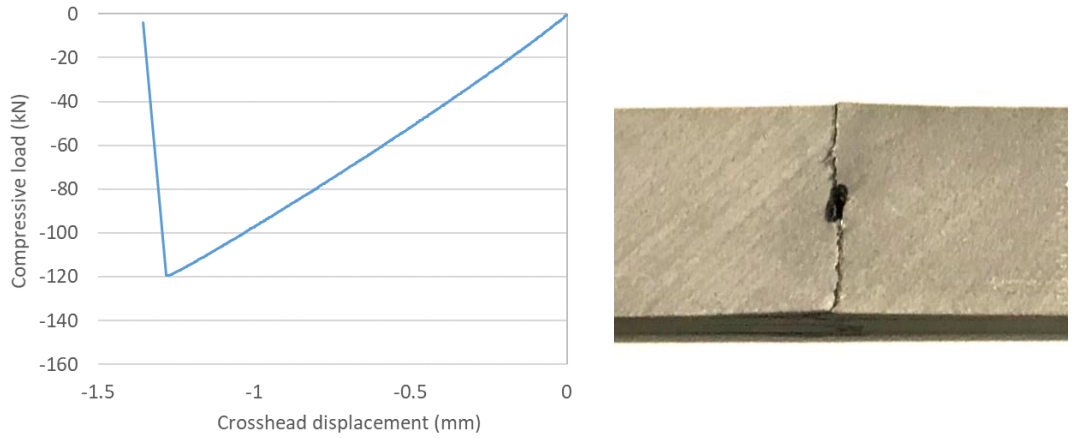

(a) A typical Scale 8 centre-notched result (C = 25.4 mm)

(b) A typical failed baseline specimen (C = 3.2 mm)

Figure 3. Typical load vs. crosshead displacement curve and fracture morphology.

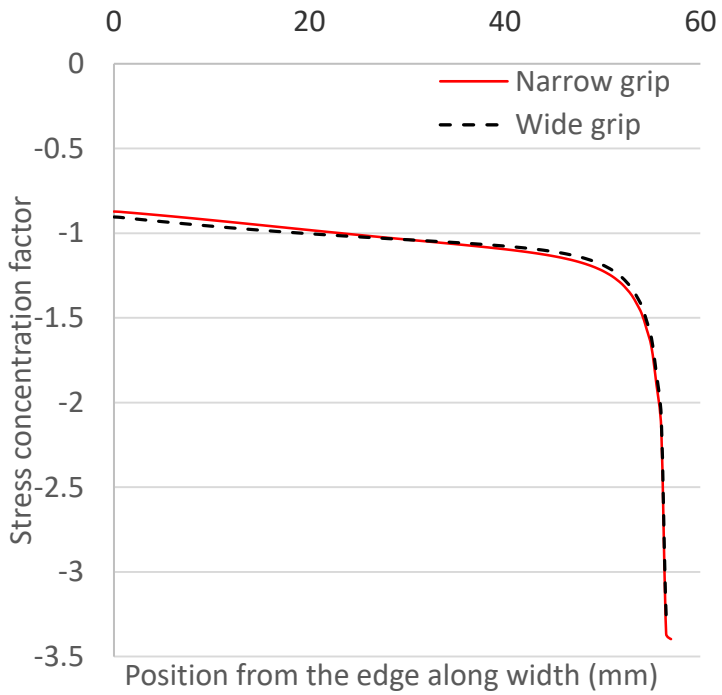

Figure 4. Stress distribution along specimen width in the simple Scale 8 centre-notched FE model (C = 25.4 mm).

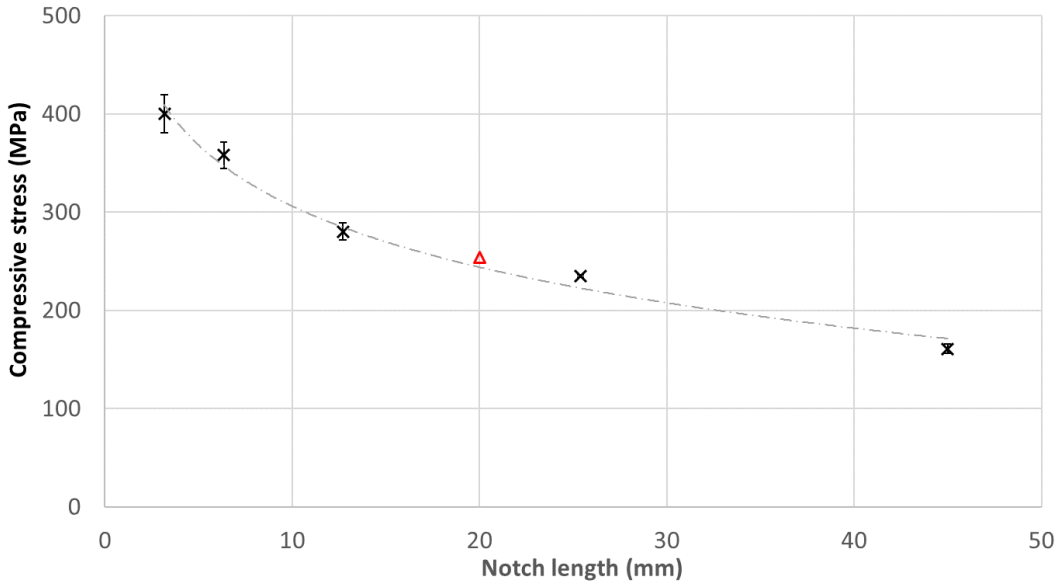

Figure 5. Verification of the Scale 8 (C = 25.4 mm) centre-notch experimental results.

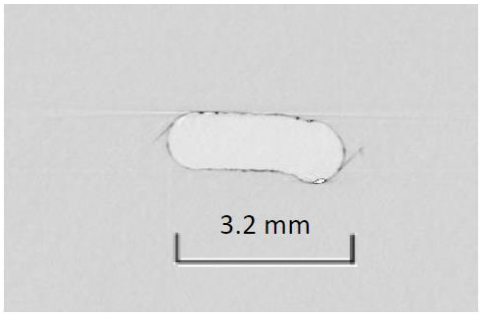

a) Typical 45° ply

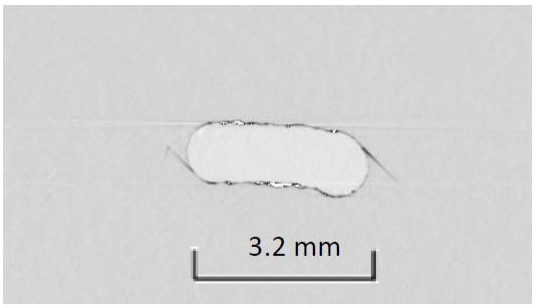

b) Typical -45° ply

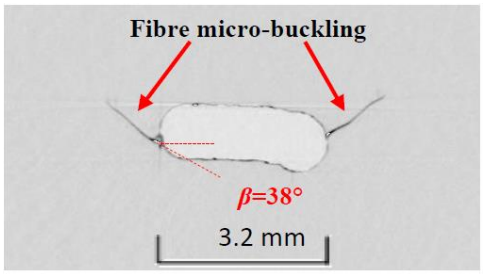

c) Typical outboard 0° ply

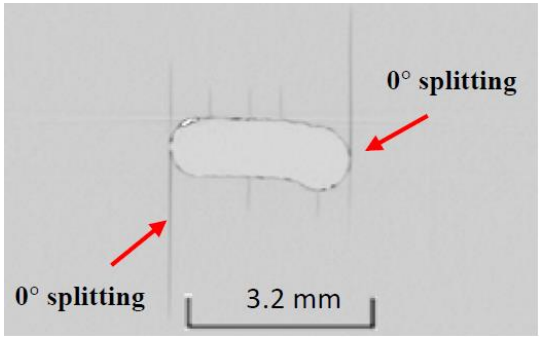

d) Double central 0° ply

Figure 6. CT Scans for the baseline centre-notched specimen (C = 3.2 mm) at about 95% the average failure load.

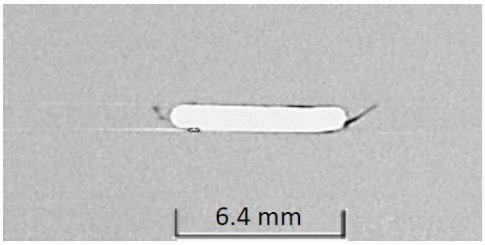

a) Typical 45° ply

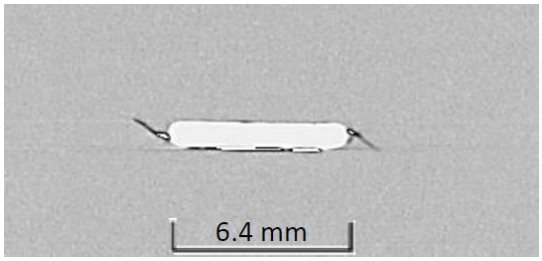

b) Typical -45° ply

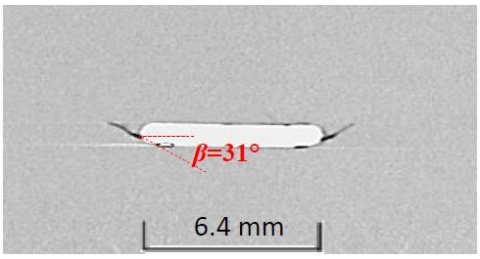

c) Typical outboard 0° ply

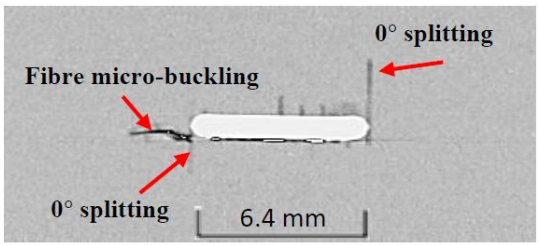

d) Double central 0° ply

Figure 7. CT Scans for the Scale 2 centre-notched specimen (*C* = 6.4 mm) at 95% of average failure load.

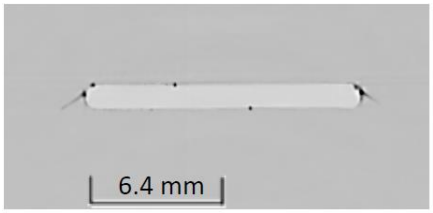

a) Typical 45° ply

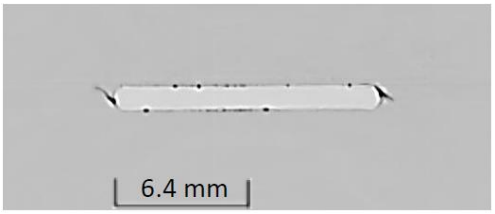

b) Typical -45° ply

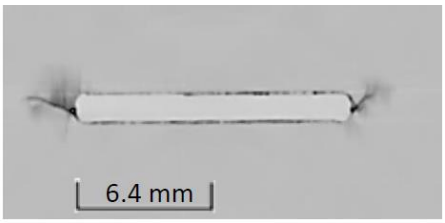

c) Typical outboard 0° ply

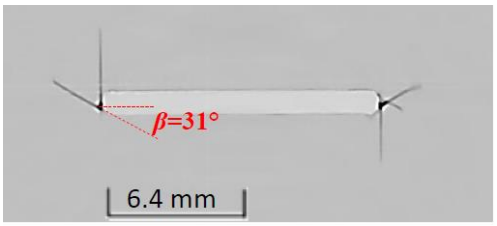

d) Double central 0° ply

Figure 8. CT Scans for the Scale 4 centre-notched specimen (*C* = 12.7 mm) at 95% of average failure load.

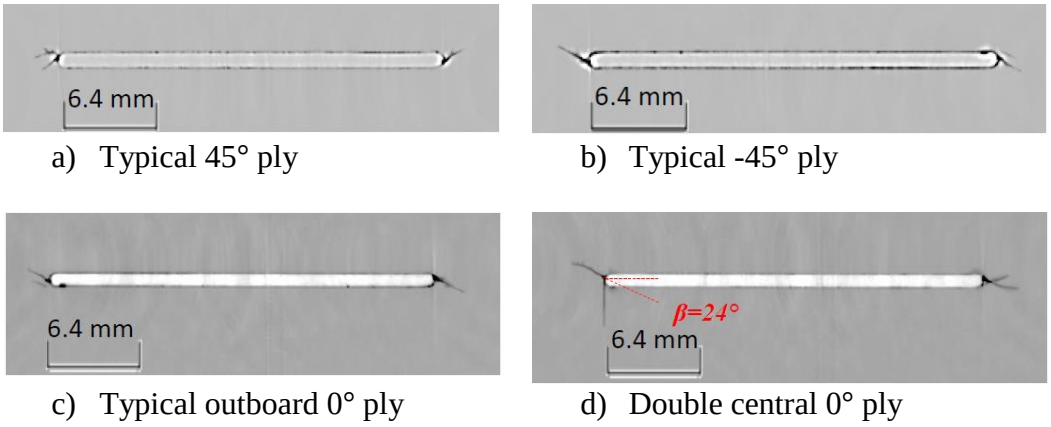

a) Typical 45° ply b) Typical -45° ply

c) Typical outboard 0° ply d) Double central 0° ply

Figure 9. CT Scans for the Scale 8 centre-notched specimen (C = 25.4 mm) at 95% of average failure load.

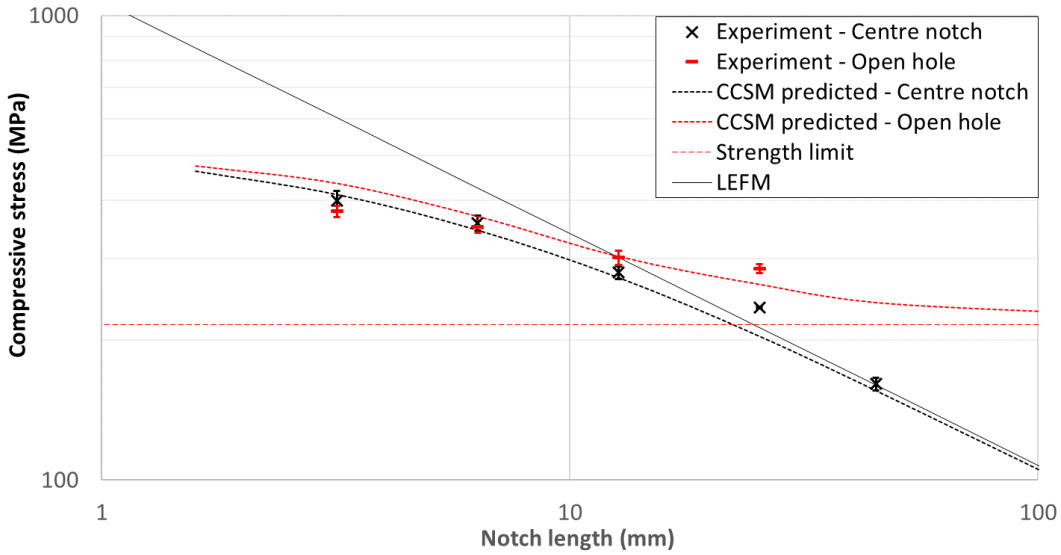

Figure 10. Scaling of notched compressive strengths.

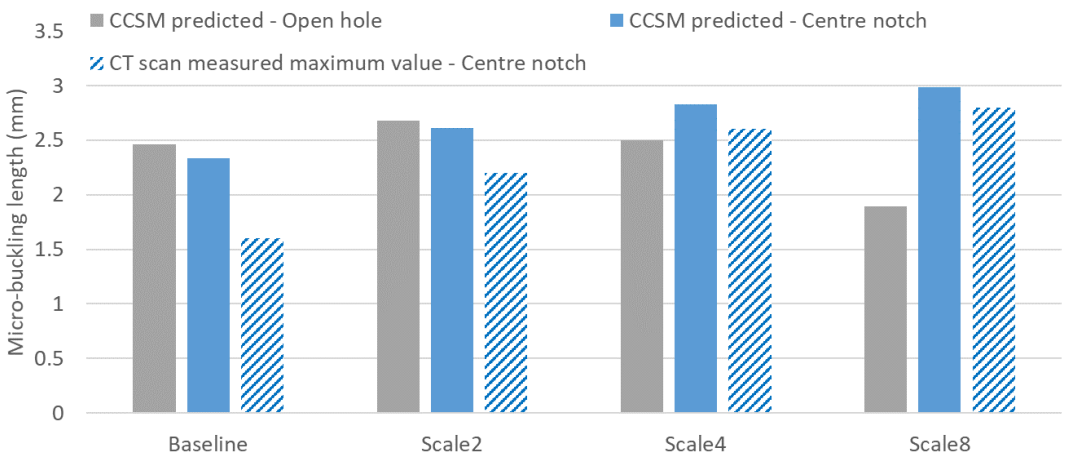

Figure 11. Comparison of micro-buckling lengths.

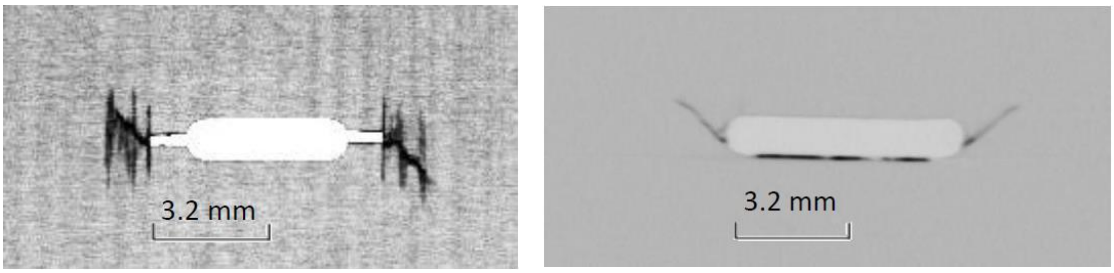

a) Tension [16] b) Compression

Figure 12. CT scans of outboard single 0° ply for Scale 2 specimens (C = 6.4 mm) under two different loading conditions at 95% of average failure load.

Table 1. Dimensions of the centre-notched specimens tested.

Specimens	**Number of Specimens**	**Notch Length, *C* (mm)**	**Gauge Width, *W* (mm)**	**Gauge Length, *L* (mm)**	**Gripping Area (mm^2)**
Baseline	5	3.2	15.9	15.9	50×15.9
Scale 2	5	6.4	31.8	31.8	50×31.8
Scale 4	5	12.7	63.5	63.5	50×63.5
Scale 6	1	20.0	100	100	100×100
Scale 8	3	25.4	127.0	127.0	100×100
Scale 14	3	45.0	225	225	-

Table 2. Experimental results (MPa) (C.V. %).

	Baseline	**Scale 2**	**Scale 4**	**Scale 8**	**Scale 14**
Notch length (mm)	3.2	6.4	12.7	25.4	45
Centre notch	400 (4.8)	358 (3.7)	280 (3.1)	235 (0.4)	161 (3.0)
Open hole	379 (2.6)	351 (2.9)[4]	300 (3.6)[4]	285 (2.2)[4]	198 (4.3)[a]

[a] Scale 14 open-hole results influenced by global buckling

Table 3. Input parameters for CCSM analysis for IM7/8552 laminates.

E_{11} (GPa)	E_{22} (GPa)	G_{12} (GPa)	υ_{12}	$QI\ \sigma_u$ (MPa)	$QI\ K_C$ (MPa·m$^{0.5}$)
161	11.4	5.17	0.320	675 [5]	43.9 [a]

[a] *K*c measured from the largest Scale 14 centre-notched tests